Landslides (2019) 16:1567–1581
DOI 10.1007/s10346-019-01205-8
Received: 9 January 2019
Accepted: 21 May 2019
Published online: 18 June 2019

I. P. Kovács · Sz. Czigány · B. Dobre · Sz. Á. Fábián · M. Sobucki · G. Varga · T. Bugya

A field survey–based method to characterise landslide development: a case study at the high bluff of the Danube, south-central Hungary

Abstract There are several common tools and practices to record surface displacement, monitor and characterise landslide development. However, is it possible to use only total station monitoring network to gain useful information for mass movement detection characterisation? In our study, we focus on the field monitoring of the Castle Hill area (south-eastern Transdanubia, Hungary) and provide a methodology to monitor and characterise displacement processes. A 5 × 5 m resolution grid network was set up to cover active and stable parts of the hill and was surveyed 27 times between 2011 and 2016 using a total station device. The total station–based monitoring network was found suitable for the detailed monitoring of the study area at a low cost, with low maintenance, quick data processing capabilities and moderate but manageable precision. Using 3D coordinates, we differentiated the individual parts of the moving block (MB), knowing that the displacements of the MB were several orders of magnitude greater than the precision of the actual surveillance method. The main displacement component (direction) was the vertical subsidence here, which was less than 4 m on the northern MB and exceeded 4 m on the southern MB. The whole MB moved to the east; however, the southern MB moved to the east 1 m shorter distance than the northern MB. *y* component movements ranged between 125 and − 271 mm over the entire MB. Small-scale displacements have been detected on the stable background (BA) using normality testing of data, and displacements were identified on the field as shallow hollows (growth cracks).

Keywords Landslide monitoring · Landslide characterisation · High bluff · Field survey

Introduction and aims

Although mass movements are one of the most hazardous geomorphic processes in Hungary (Pécsi 1994; Szabó 2003; Lóczy et al. 2007), monitoring data on movement rates and trends are scarce (Kovács et al. 2015); thus, detailed characterisation of mass movements is unavailable. As the high bluffs are often covered by dense vegetation and displacements are relatively small (hundreds of metres), the number of applicable data collection techniques is limited here.

There are several common tools (Angeli et al. 2000) and practices (Maček et al. 2014) with advantages and disadvantages (Savvaidis 2003; Liu and Wang 2008; Arbanas and Arbanas 2014) to record surface displacement, monitor and forecast landslide susceptibility (Guzzetti et al. 2005; Reichenbach et al. 2018) and development. Common practices such as levelling, total station measurements (Carlà et al. 2018), GPS surveys (Guerriero et al. 2018), inclinometer and extensometer measurements (Garcia et al. 2010), LIDAR (Jaboyedoff et al. 2012), terrestrial laser scanning (Huang et al. 2018), geomorphological mapping (Guzzetti et al. 2012), GB-InSAR, InSAR, terrestrial and aerial photogrammetry (Zhao and Lu 2018), UAV (Peppa et al. 2016; Casagli et al. 2017; Hu et al. 2018) and UAV combined with RTK (Mozas-Calvache et al. 2017) may differ in accuracy, applicability (Chae et al. 2017; Pecoraro et al. 2018) and also in cost-effectiveness (Uhlemann et al. 2016). Despite the high number of available techniques, it still remained uncertain whether a single-sensor/instrument method is applicable to obtain useful data in a cost-effective way.

According to van Westen et al. (2008) and Corominas et al. (2014), regularly repeated theodolite measurements are highly applicable for data collection at sufficiently detailed levels, however, less appropriate for the monitoring of large areas. Using monitoring networks for data collection on a landslide is considered challenging at a local scale and possibly on site-specific level as well. The sight precision of theodolite may achieve 1 arc sec (0.15–0.3 mgon) under ideal conditions (Grist 1991; Bas 2000) while the accuracy of distance measurements is typically ± 1 mm. Nonetheless, precise levelling provides more accurate data than theodolite surveys (Savvaidis 2003); still, theodolites are sufficiently precise devices to detect seasonal oscillations of the topsoil (Carr and Blackley 1986; Bugya et al. 2011). Moreover, the presently surveyed phenomenon has a minimum order of magnitude with greater displacement detection accuracy than theodolites.

Our research is phrased to identify the capabilities of a theodolite based on displacement monitoring network, which may serve as a base for movement predictions in the future. Considering the aforementioned features of the available monitoring techniques, the following questions have been formulated:

(i) Could a total station–based network, designed for a monitoring period of several years and with measurement intervals of 1 to 2 months, provide data with sufficient precision to track landslide development for a small vegetated area? (ii) Could the collected data be sufficient (in terms of resolution of the network and data precision) for the prediction of future displacements? (iii) How can data be analysed for the aforementioned purposes? (iv) What operational experiences could be gained during the maintenance of the network (sustainability, cost- and time-efficiency and field experiences)?

Site description

Several papers have been published from the research site during the last decades, where geological (Újvári et al. 2014) and geomorphic (Újvári et al. 2009; Bugya et al. 2011; Szalai et al. 2014a, b; Kovács et al. 2015, 2018, 2019) features of the study area have been described in detail. Therefore, we provide only a short overview of the investigated site.

Rolling hills with gentle slopes formed at an elevation of 120 to 140 m a.s.l. and loess plateaus are typical landscape elements of the south-western part of the Pannonian Basin. Our study area (Castle Hill, Dunaszekcső) lies on the eastern edge of this hilly region, on the right bank of the Danube, where the southernmost high bluff

was formed by the river (Fig. 1). The Castle Hill (46° 05′ 18.4″ N, 18° 45′ 42.9″ E) lies on the top of this bluff (Pécsi 1994; Lóczy et al. 1989, 2007). The relative height difference between the hilltop and the Danube reaches 60 m (Moyzes and Scheuer 1978), while water level fluctuations can reach 10 m here.

The building materials of the bluff are composed of several sediment layers. The upper ca. 57 m of the whole section belongs to Pleistocene 'young loess' layers (Újvári et al. 2014), which are interlayered by 14 paleosoil layers and one sandy interbedding. The underlying Pliocene and Miocene sediments (ca. a 40-m-thick section) are built up of sandy silts and clays (Pécsi and Schweitzer 1995). There is no evidence of fault lines or tectonically active faults in the broader vicinity of the Castle Hill (Joó 1992).

Due to the lateral erosion of the river (bank erosion, undercutting), mass movements have been present along the bluff since historic times (Lóczy et al. 2007; Kovács et al. 2015). Therefore, the chosen test site at the Castle Hill was set up to provide an ideal spatial coverage for modelling present-day mass movements. The last large-scale mass movement occurred in 2008 here (Újvári et al. 2009). Recent landslide activity is connected spatially to the edge of the loess bluff, and it also affects the connected riverbed. Although observable at low water levels, the uplift of the riverbed, triggered by mass movements, has not yet been surveyed. Several authors have already attempted to monitor the dynamics of the bluffs (Újvári et al. 2009; Bugya et al. 2011; Kovács et al. 2015) and kinematics (Pécsi 1994; Fodor and Kleb 1994; Bányai et al. 2014) or to identify the triggering factors (Moyzes and Scheuer 1978; Kertész and Schweitzer 1991; Szabó 2003; Lóczy et al. 2007; Újvári et al. 2009, Bányai et al. 2014). Owing to its geological structure, in a hydrological sense, the Castle Hill is not an independent unit, as its groundwater table depth and soil moisture dynamics are directly related to the water regime of the Danube. Many authors, e.g. Újvári et al. (2009) and Bányai et al. (2014), claimed that the water levels of the Danube play a crucial role on the generation of mass movement processes in the area. The former dispatched blocks prevent the lateral erosion exerted by the Danube; hence, presumably, the main triggering factor is the groundwater which closely correlates with the water level of the Danube, and therefore water level in the river directly regulates the groundwater table depth of the adjacent areas (Bányai et al. 2014).

Nevertheless, the influences on displacements and fissure formations remain debated. In the current paper, we exclusively focused on the monitoring and characterisation of displacements; therefore, the role of triggering factors is neither discussed nor analysed hereby.

Methods

Field survey

The former monitoring network, established by Bugya et al. (2011) in 2009, was extended in October of 2011. The new grid network (Fig. 2) was based on the base points of the former network with a resolution of 5 × 5 m. The geographical positions of the 89 survey points of the grid network were established with a Sokkia SET 630RK total station. Points were marked both on the active part and the stable part of the high bluff (both to the east and west from the continuously developing crack). Thus, the investigated area covered the new active slump block (zone of slope failure) and a 15- to 20-m-wide zone of the stable surface, with the exception of buildings and dense vegetation. The abovementioned spatial setting of points provided the base to compare the processes of the background (BA) and the actively moving landslide. The northwestern part of the survey network was extended to the west (13 new points were added) in December of 2011 (field campaign 3), due to the growth of the developing crack. The survey points were fixed with steel rods of 1 m long and 10 mm in diameter into the ground, to prevent their displacement caused by seasonal frost events and a ground motion reported by Bugya et al. (2011) in the area formerly.

The base point (Alo) of the grid network was established on the westernmost part of the high bluff. This location was an optimal viewpoint for the optical measurements and is unaffected by displacements. Comparing the location of the base point to the moving slump block, there were no geomorphic evidences of active displacements at a distance of 30 m from the base point. Hence, this location provided a base of relative stability for the measurements. The point was also marked with a metre-long steel rod and a concrete shell of 10-cm diameter within a plastic tube to fix the position of the base point. A secondary (reference) point was marked on the top of a water tank. Hence, the reference point stayed at a distance of 15 to 20 m from the active fissure, and the concrete walls of the water tank maintained a long-lasting stability for the reference point. The original base point of the grid network was damaged in March of 2016; hence, the base point of the former network established by Bugya et al. (2011) was used instead as a base point for subsequent measurements.

Absolute geographic coordinates of the base and secondary base point were measured with a Topcon Hiper Pro differential GPS (DGPS). DGPS measurements were taken with an accuracy of 5 mm, based on a point of national geodetic network at Dunafalva (left bank of the Danube). Base and reference points were used to orientate the measuring device. First, the total station was oriented in east-west (x) direction then north-south (y), and vertical (z) coordinates of the marked points of the network were measured during each field campaign. The reference point was measured again at the end of the survey to obtain information on inaccuracies accumulated during the campaign. Despite the measured real geographic coordinates of the grid network points, we only determined their relative movements, measured by the total station, due to the low precision of the aforementioned DGPS measurements. However, spatial development of the crack network was regularly recorded using repeated photo documentation and occasional DGPS surveys.

Twenty-one periodic field surveys have been executed at regular 1-month intervals between October 2011 and January 2014, and a last control measurement was taken in March 2015 (Fig. 3). Measurement campaigns were restarted in November 2015 and were ongoing until October 2016, with measurement intervals of 2 months. Altogether 27 measurements were taken during the 1850 days of the field monitoring. Due to the difference in measurement intervals, data were analysed separately from October 2011 to March 2015 (campaign period 1) and between November 2015 and December 2016 (campaign period 2).

Data analysis

Considering the measured displacements of the research area, different data processing methods were applied on the BA and

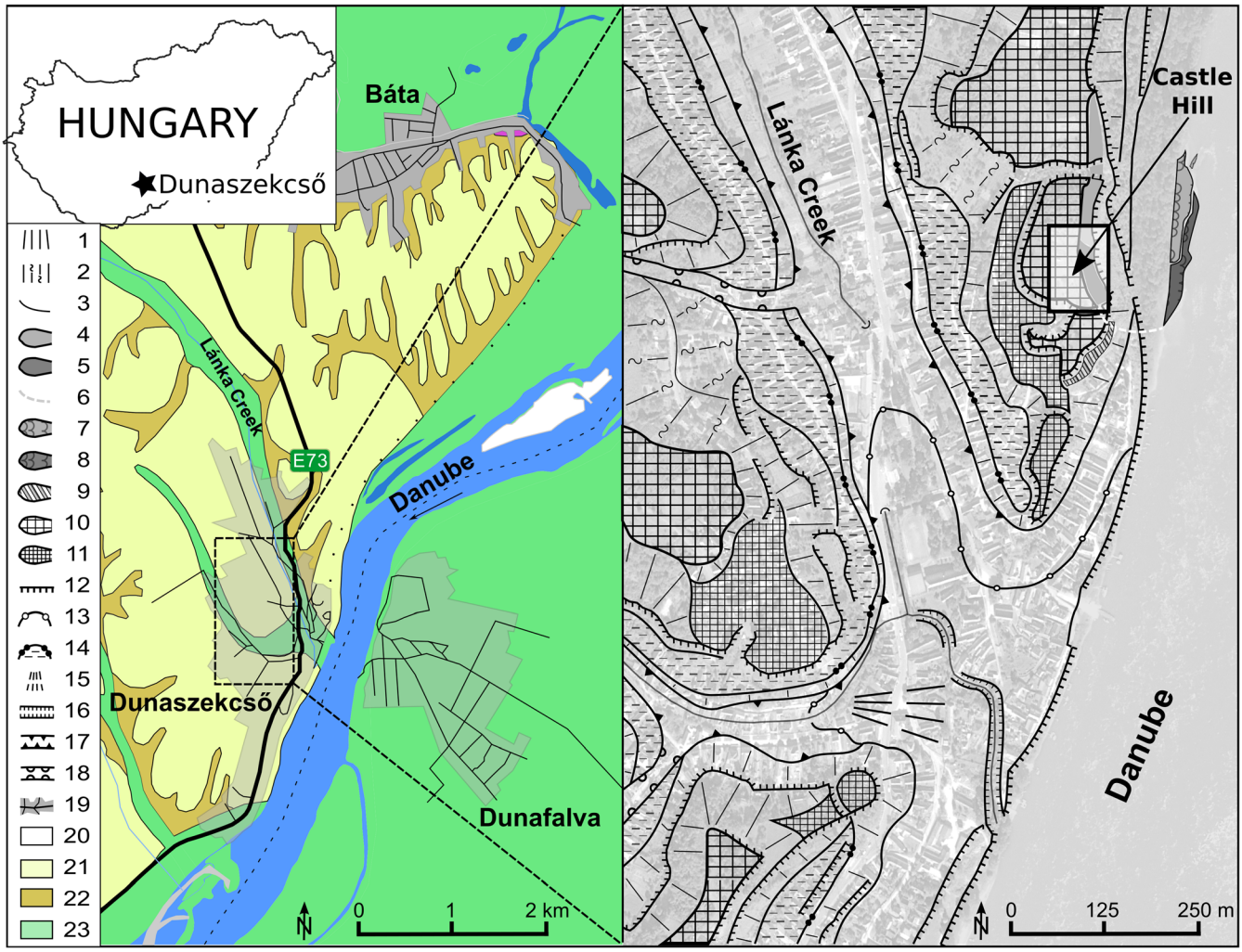

Fig. 1 Site location and geomorphological sketch of Dunaszekcső. 1 = stable slope; 2 = unstable slope; 3 = general change in slope angle; 4 = landslide head in 2008; 5 = active landslide head since 2011; 6 = side crack of the recent landslide; 7 = peninsula in 2008; 8 = peninsula after 2011; 9 = retaining wall; 10 = loess plateau; 11 = lower surface; 12 = anthropogenic terrace; 13 = floodplain; 14 = terrace; 15 = alluvial fan; 16 = artificial channel; 17 = erosional valley; 18 = dry valley; 19 = residential area; 20 = research area; 21 = Middle Pleistocene loess; 22 = Late Pleistocene-Holocene proluvial and deluvial sediments; 23 = Holocene fluvial sediments (geological features are according to Franyó et al. 2005)

on the moving block (MB). Firstly, *x*, *y* and *z* displacement components were calculated for each point on the MB for each campaign data using the first campaign as a zero measurement. Cumulative displacements were mapped until the end of measurement campaigns 1 and 2 according to displacement components. Secondly, empirical probability density functions (histograms) were built for relative *y*, *x* and *z* displacement values of each survey point separately. Interval (class) widths on histograms were also determined in respect of the precision of the survey method. The precision of the total station ranged between ± 5 mm (Sokkia SET 630 RK user guide); therefore, a class width (10 cm) of an order of magnitude higher was applied to account for device imprecision. Histogram bins represent the observation number of displacements at a certain displacement range. However, the number of classes also describes the temporal pattern of movements. Survey points were clasterized based on their patterns of the histograms of their displacement components using visual interpretation to spatially and temporally separate a uniform part from the MB. Low numbers of histogram classes close to the zero value of the histogram suggest low magnitude of displacements, while the appearance of individual classes describes further movement phases. Clusters were mapped applying gradual colour tables, where light yellow colour indicates clusters with a single movement type and red colour highlight cluster was used where the numbers of displacement phases were the highest.

According to our former field survey, the background area was considered stable; methods used for the MB were not applicable here. We assumed that in the case of complete stability of the background area, measured relative displacements should represent zero movements and detected movements only reflect measurement inaccuracies. Therefore, we assumed normal distribution here; otherwise, the non-normal distribution indicates actual displacement. Using the Kolmogorov-Smirnov analysis (Lilliefors 1967), we have tested the similarity of displacement patterns to normal distribution. The statistical pattern of the survey points was calculated using

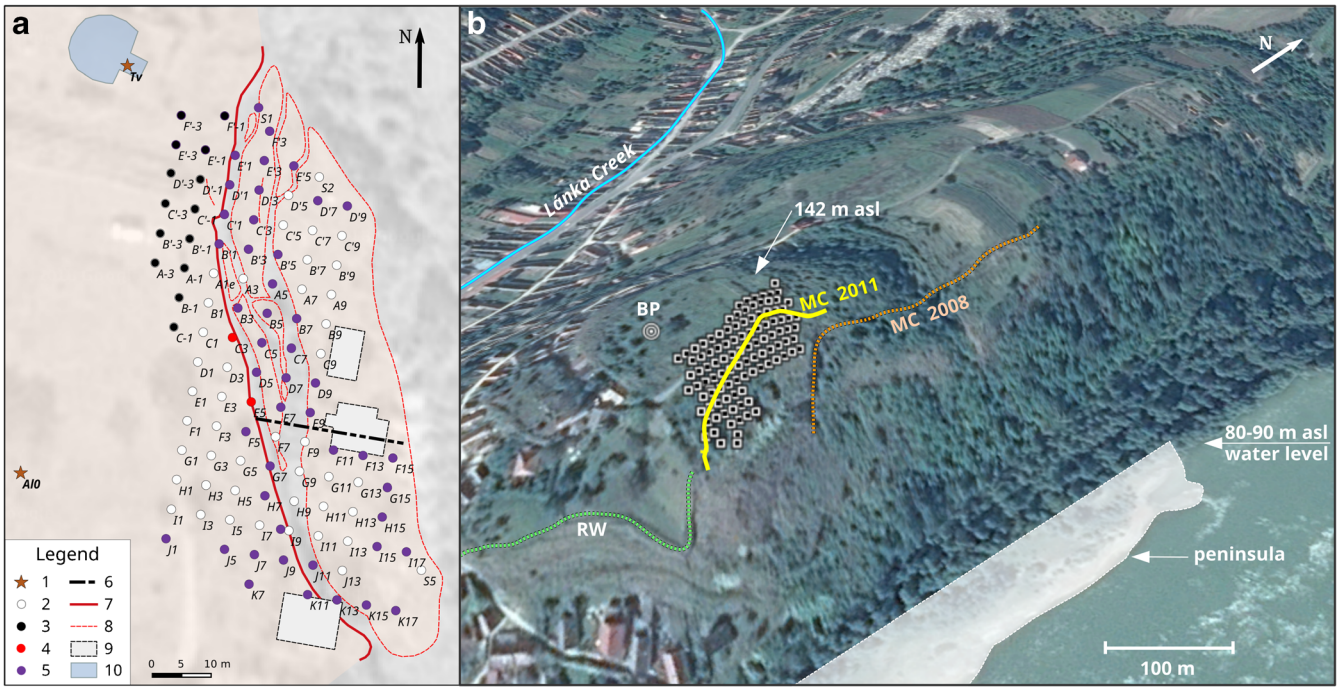

Fig. 2 **A** Sketch of the monitoring network. AI0 = base point; Tv = secondary base point; 2 = survey point; 3 = survey point established during measurement campaign 3; 4 = survey point lost until measurement campaign 22; 5 = survey point lost between measurement campaigns 22 to 27; 6 = border of the northern and southern parts of the MB; 7 = main crack (MC); 8 = bolder of the surface fragments on the MB; 9 = buildings; 10 = water tank. **B** 3D model of the research area. BP = AI0 (base point), MC 2008 = main crack from 2008; MC 2011 = main crack from 2011; RW = retaining wall

Gnumeric Spreadsheet 1.12.28. software, and data were mapped and further analysed in Qgis 2.14.3. and OpenOffice.org 4.1.1.

$$D = \max_x \mid F^*(x) - S_N(x) \mid,$$

where N is the number of observations, $S_N(x)$ is the sample cumulative distribution function, $F^*(x)$ is the cumulative normal distribution function with $\mu = \bar{x}$, the sample mean, and $\sigma^2 = s^2$, the sample variance, defined with denominator $n - 1$.

Several points turned unmeasurable during the surveys mainly due to the development of the crack network (along the main and adjacent cracks) and partly due to rockfalls and changes in the vegetation on the edge of the point network. These points did not enable further accurate surveys on the deformations but provided useful data on the development of the fissure network. Hence, measured data of all survey points have been integrated into the same database; however, unmeasurable points were not further analysed.

Results

Displacements of the BA

The BA remained unchanged during the entire period of the survey, while clearly visible displacements of several metres were detected on the MB. Displacements on the BA did not exceed 29 mm in any (x, y and z) directions, and the majority of the relative point positions were fluctuating between 0 and ± 10 mm (1/a, b and c on Fig. 4). Displacements, larger than 10 mm were observed only on the northern part of BA during the last campaigns. The total length of the absolute displacements between the first and last campaigns did not reach 30 mm on the slump block stable background area (SB) over the survey period of 1850 days. Point velocities were also less than 0.01 mm/day; only one single point reached a velocity of 0.02 mm/day over the entire survey period. Furthermore, azimuthal direction and the dip angle of block heads varied greatly here. Due to the replacement of the original base point with a new one in March 2016, a decrease in measurement accuracy was observed. Therefore, the standard deviation of x, y and z values of measured points slightly increased until the end of campaign period 2.

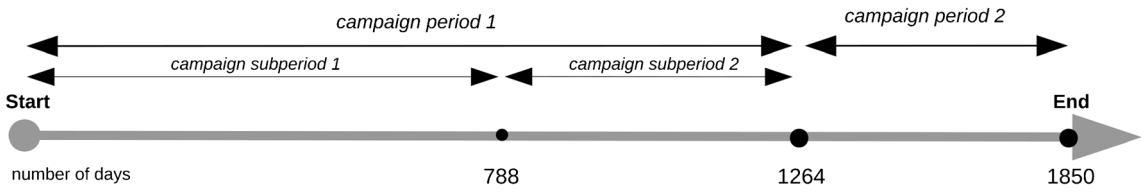

Fig. 3 Timescale of the field campaigns

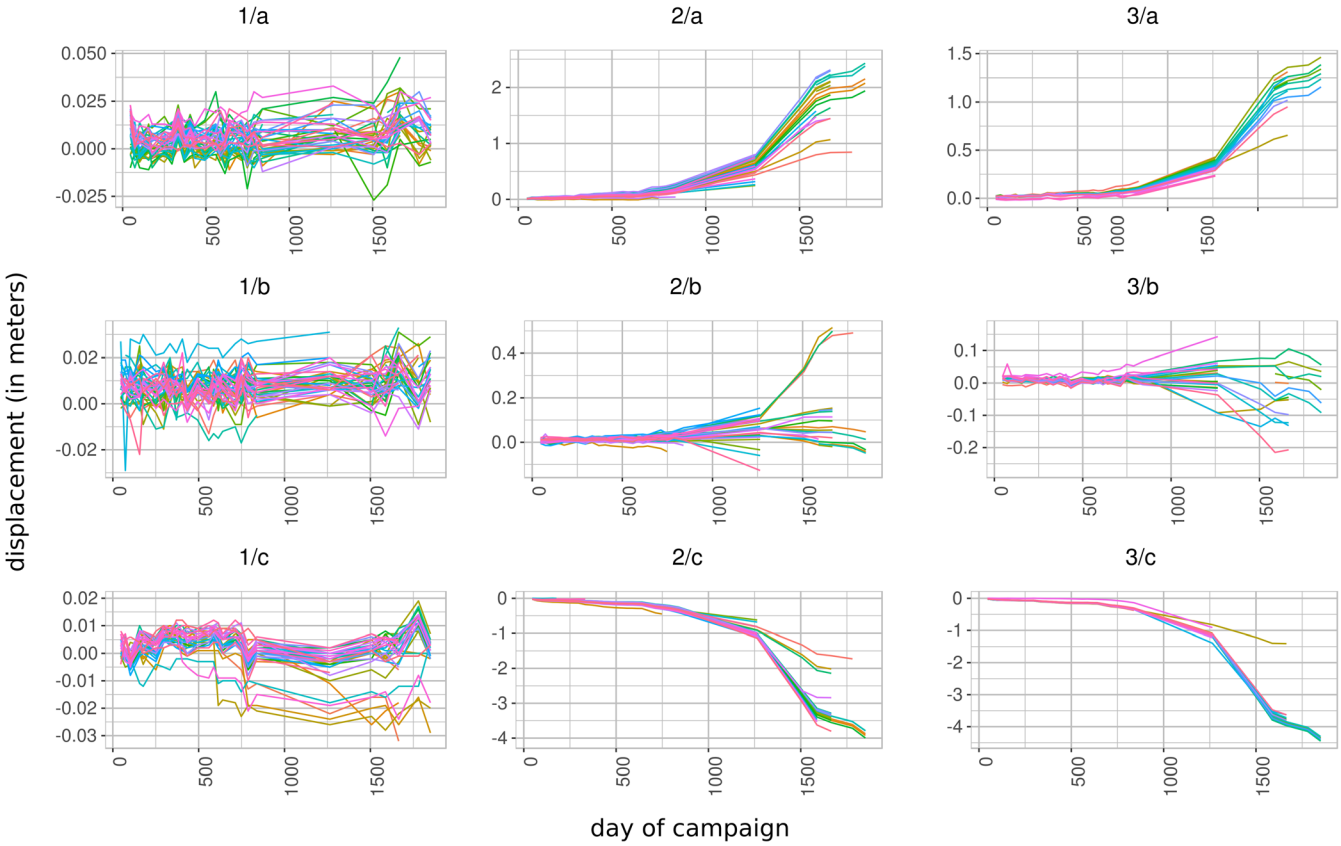

Fig. 4 Displacements of survey points. Column 1 = points of the SB. Column 2 = points of the northern MB. Column 3 = points of the southern MB. 1 = x component of displacements. 2 = y component of displacements. 3 = z component of displacements

Displacements on the MB during the campaign period 1

Horizontal and vertical positions of the MB points have changed in time (2/a, 2/b, 2/c and 3/a, b, c on Fig. 4). Over field campaign subperiod 1, i.e. between days 1 and 788 (field campaign 20), the MB points moved with relatively low velocities, and displacements had clear linear trends. The field campaign subperiod 2 covered campaigns 20 and 22 (day 789 to day 1264), during which displacements have been accelerated and larger-scale movements led to visible surface changes (Fig. 5).

During field campaign subperiod 1, the x component movements of the MB varied between 238 and 25 mm (A on Fig. 6). x values decreased steadily to the south and from the east to the west on the MB. This trend indicated that the northern and eastern parts of the MB moved away from the main crack (MC) to a greater extent than the southern part of the MB. The north-south movement component (y) ranged between 53 and −3 mm (B on Fig. 6). y values increased toward the MC, demonstrating that points close to MC moved toward the north faster than the ones located further away. Vertical displacements (z) ranged between −344 and −2 mm (C on Fig. 6). Z values increased to the direction of the MC and to the north-western part of MB, indicating greater subsidence rates there.

The only visible change was the gradual opening of the MC along the western part of MB during field campaign subperiod 1. The opening was only detectable on the surface on the northern MB during early measurements. The southern part of the escarpment remained covered until the end of the field campaign subperiod 1 due to plastic behaviour of the topsoil. Despite the displacements of only a few tens of centimetre, MB was clearly separated from the BA. Moreover, MB seemed uniform without any further intrablock (minor scarp) development and displacements.

During field campaign subperiod 2, x component movements of the MB varied between 605 and 204 mm. x values decreased steadily to the south and low values occurred near the MC, which means that the southern MB moved to the east with lower velocity. y component ranged between 109 and −146 mm. y values increased to the direction of the MC and to the northernmost part of MB. Negative values occurred in the western-central section of the MB and on the eastern edge of the southern part of MB; hence, these points moved to the south, while the rest of the MB moved to the north. z values ranged between −1102 and −322 mm. z value–indicated subsidence was more intense on the eastern edge of the northern part of MB and the western edge of the southern part of the MB. Dissection of the northern MB (scarp development) started in the campaign subperiod 2, and scarps became visible due to the accelerated displacements. Scarps developed from the north to the south on the northern MB, simultaneously with the opening of the MC. However, despite of the accelerated velocity of movements, vertical differences reached only less than 1 m on the northern MB. The behaviour of the southern MB looked

Fig. 5 Displacements, growth cracks and scarp development along the crown of the MB. **A**–**D** Southern MB. **E**–**H** Northern MB (pictures were taken from the south toward north). **A**, **E** = field campaign 1; **B**, **F** = field campaign 20; **C**, **D** = field campaign 22 (end of campaign period 1); **D**, **H** = field campaign 27 (end of campaign period 2)

unchanged compared with field campaign subperiod 1; however, the subsidence rates in the southern MB were clearly faster than in the northern MB.

Displacements on the MB during the campaign period 2

During the campaign period 2 (days 1265 to 1850, field campaigns 23 to 27), the formerly observed movement tendencies continued, and at the same time, the subsidence rates of the MB rapidly increased. At the beginning of campaign period 2, 63 points were available on the whole research area and 27 were measurable on the MB. The main reasons for the loss of points were the large-scale surface and vegetation changes.

x component movements of the MB ranged between 1805 and 717 mm (A on Fig. 7). *x* values decreased from the north to the south and from the east to the west. Hence, the northern and western parts of the MB were sloping to the east, but other parts of the MB were displaced to the opposite direction. *y* component values ranged between − 234 and 23 mm (B on Fig. 7). Negative *y* values indicate that the whole MB moved to the south, except the points located in the close proximity of MC. Moreover, faster

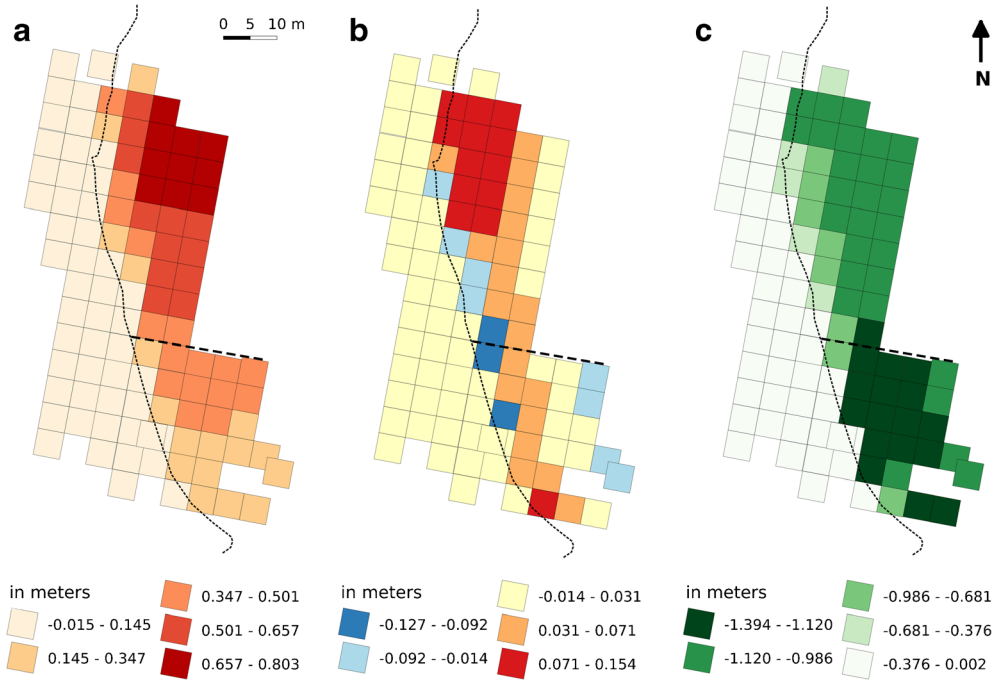

Fig. 6 Measured displacements during the campaign period 1 (field campaigns 1–22) in metres. **A** *x* displacement component. **B** *y* displacement component. **C** *z* displacement component. Dashed line indicates the border of southern and northern. To identify additional geomorphic details of the monitoring network, see Figs. 2B and 5D and H

southward movements were observed on the southern MB, while its northern part was displaced at a relatively low rate. *z* values fluctuated between −3253 and −2649 mm (C on Fig. 7). Subsidence was more intense on the southern part of the MB than in its northern segment. However, the eastern part of the northern MB subsided more rapidly than its western part.

Due to the more intense displacements, dramatic surface changes were found during the campaign period 2. On the northern MB, three large and several small internal slump blocks were separated by cracks and scarps with their axis parallel with the MC. Their southern end disappeared at the point named F7, west of the abandoned house. The widths of the large internal blocks were up to 5 to 10 m; however, the width of smaller internal blocks was less than 3 m. Their height reached 1.5 to 2 m until the end of campaign period 2. The southern part of the MB uniformly subsided by up to 4 m. Its western part had a lower subsidence rate, since it collided with the scarp of the MC; thus, a few metre-wide fragments were separated from the MB.

Cumulative displacements during campaign periods 1 and 2

In the following paragraph, we compare displacement parameters over the entire field survey (between campaigns 1 and 27). About 50% of the measured points have been lost and/or become unusable during the 1850 days of the monitoring campaign, due to the accelerated movement of surface displacements (crack development) and the growth of the vegetation (Fig. 8). More than 20% of the total of point losses occurred between field campaigns 22 and 23, and the same percentage of survey points became unusable by campaign 25. Despite the massive loss of points, maps comparing the data obtained during the first and last field survey provide useful information on the overall dynamics of the landslide.

x component movements of the MB ranged between 2541 and 27 mm. The whole MB moved to the east; however, eastward movements on the southern MB were about 1 m shorter than on the northern MB. *y* component movements ranged between 125 and −271 mm over the entire MB. The eastern edge and the entire southern part of the MB were moved to the south. *z* values of the MB were ranged between −3686 and −4451 mm. On the northern MB, a subsidence of less than 4 m was detected, while subsidence exceeded 4 m on the southern MB.

The length of displacements calculated from *x*, *y* and *z* reached 1.7 to 2.5 m in the northern MB and 1 to 1.5 m in the southern MB. Only a few extreme displacement values, caused by crack openings and development, were measured on the MB.

Velocity values ranged between 1.3 and 0.4 mm/day in the MB; however, values of 1.3 to 0.9 mm/day and 0.8 to 0.4 mm/day were measured on the northern and southern MB, respectively (A on Fig. 9). Strong north-north-western and south-south-eastern ramps were observed along MB, considering the intensity of displacements. The slope gradients of the displacements varied between 51 and 66° on the northern MB and between 62 and 76° on the southern MB in respect of the local horizontal level (B on Fig. 9). Azimuthal direction of displacement vectors ranged between 87 and 91° on the northern MB and 88 and 95° on the southern MB.

Cumulative displacements during campaign periods 1 and 2 based on the spatial distribution of the survey points

Background area

Despite the presumed stability and measured low values of point displacements, only a few points had normal distribution among all movement directions (Fig. 10). The majority of the points with

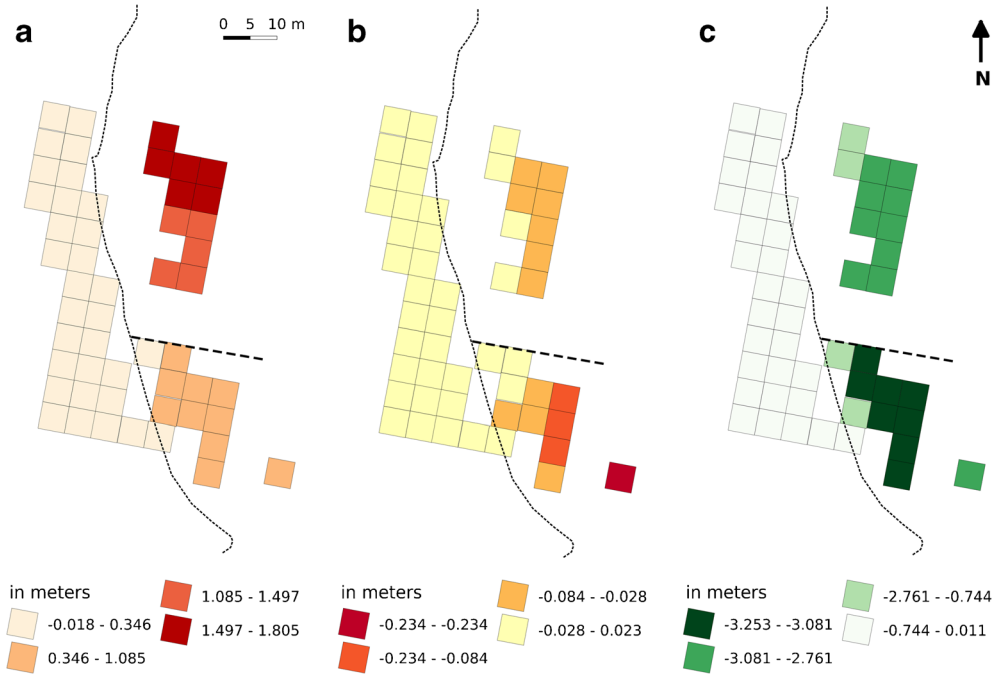

Fig. 7 Measured displacements during campaign period 2 (field campaigns 22 to 27) in metres. **A** *x* displacement component. **B** *y* displacement component. **C** *z* displacement component. Dashed lines indicate the border of southern and northern MB. To identify additional geomorphic details of the monitoring network, see Figs. 2B and 5D and H

normal distribution were detected for the *y* component (A on Fig. 10). In contrast, the number of non-normal distributions was much higher for the *x* and *z* components. In the case of the *y* component, a few points with non-normal distribution were found isolated on the southernmost and northern parts of BA and close to the MC (B on Fig. 10). In the case of the *x* component,

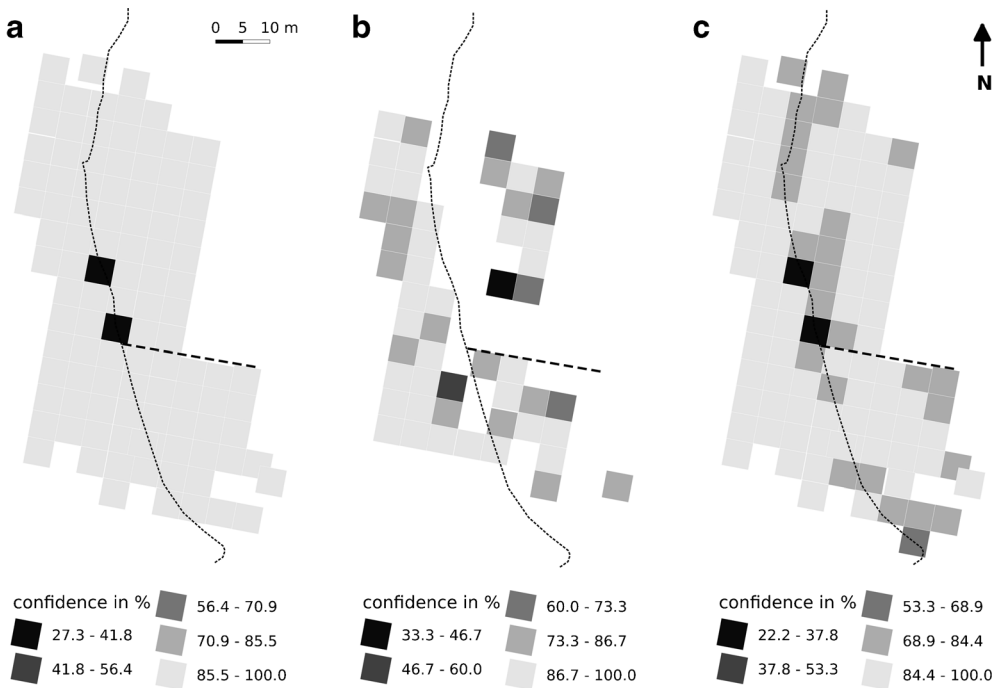

Fig. 8 Confidence of the measuring points in percentage (%). **A** Campaign period 1 (field campaigns 1 to 22). **B** Campaign period 2 (field campaigns 22 to 27). **C** All campaign measurements. Dashed line indicates the border of southern and northern MB. To identify additional geomorphic details of the monitoring network, see Figs. 2B and 5D and H

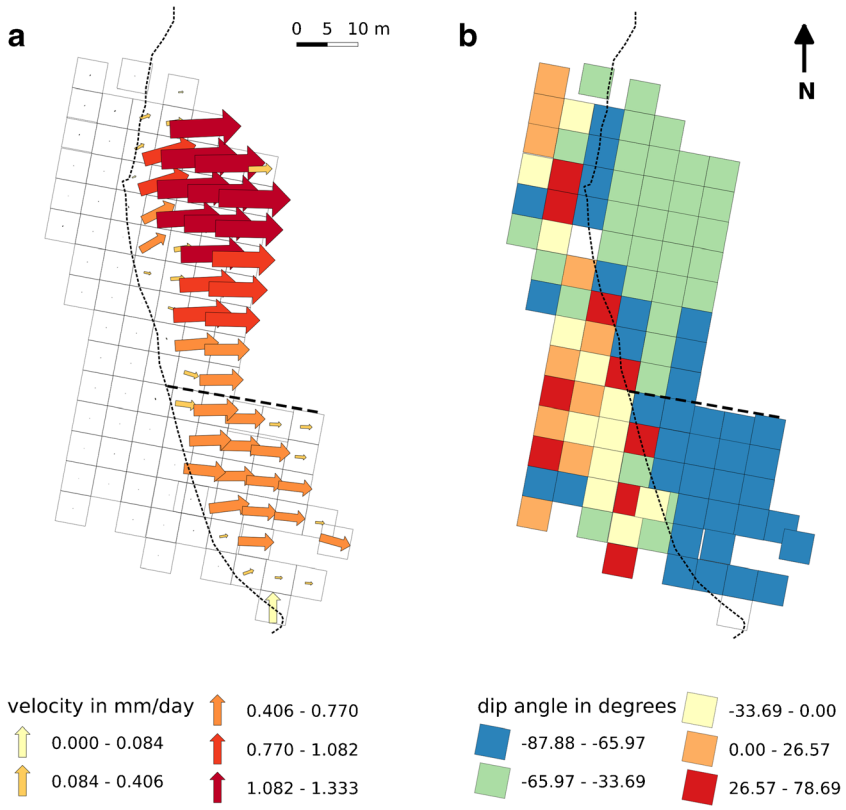

Fig. 9 Velocities, movement directions and dip angles of measured displacements during the monitoring campaigns. **A** Velocity and direction of displacements (mm/day). **B** Dip angle of real displacement. To identify additional geomorphic details of the monitoring network, see Figs. 2B, and 5D and H

two spatial concentrations of points with non-normal distribution were found in the centre and in the south-central part of BA. On the contrary, almost all points of the BA demonstrated non-normal distribution, only the *z* values of the westernmost points were nearly normally distributed (C on Fig. 10). Notable coincidence is that two new shallow and up to 7- and 4-m-long hollows (juvenile growth cracks) were detected in October 2018 at the north-eastern edge of BA, having parallel axes with the MC (Fig. 11). The northern one (NH1/a on Fig. 11) was up to 20 cm deep and reached a width of 2.5 m, while the southern one (NH1/b on Fig. 11) had a depth of 15 cm deep and a width of 0.5 m. Another growth crack (NH2 on Fig. 11) appeared on the southern part of BA and reached a depth of 20–25 cm and had an area of 5 × 7.5 m.

MB

Histograms of the measured points of the MB were grouped into 5 classes according to the displacement heterogeneity of the *x*, *y* and *z* components of each point (Figs. 10 and 12). Regarding the *x* displacement component, we experienced larger heterogeneity of displacement clusters, on the northern MB, while the southern MB indicated less frequent changes (higher level of uniformity) in eastward movements. Repeated movements were concentrated on the western and north-eastern parts of the MB. Considering the spatial variations of *y* component clusters (B on Fig. 10), the MB showed a spatial duality with frequent displacements on the southern and northern MB and a zone of low magnitude of *y* displacements between the northern and southern MB.

The spatial distribution of the *z* displacement clusters (C on Fig. 10) was similar to the spatial pattern of the *x* clusters (A on Fig. 10). The southern MB showed a higher level of uniformity, while the northern MB had a rather mosaic pattern.

Discussion

Despite the loss of marked geodetic points by field campaign 27, it was possible to detect ongoing slope failures, the development of the MB and the fissures along the escarpment. The loss of measurement points by the end of the campaign period 2 had two contradictory effects. Firstly, the lower number of geodetic points hindered the interpretation of both the spatial and temporal patterns along the escarpment. Secondly, point loss provided revealed valuable information on the development of the fissure network.

The spatial resolution of the current survey was lower than the resolution of the former precise levelling results (Bugya et al. 2011) but much higher than the resolution of the GPS surveys by Újvári et al. (2009) and Bányai et al. (2014). Temporal resolution of the measurement intervals (field campaigns) was sufficient to detect the abovementioned details of the displacements. Further enhancing the temporal resolution (measurement campaigns of shorter return periods) would lead to more detailed surveillance data of the slope failures in the area. However, measurements with lower temporal resolution (measurement intervals of 2 to 6 months) could also deliver valuable information; hence, frequent measurements are not crucial, since the main features and slope deformation trends have already been identified by former field observations.

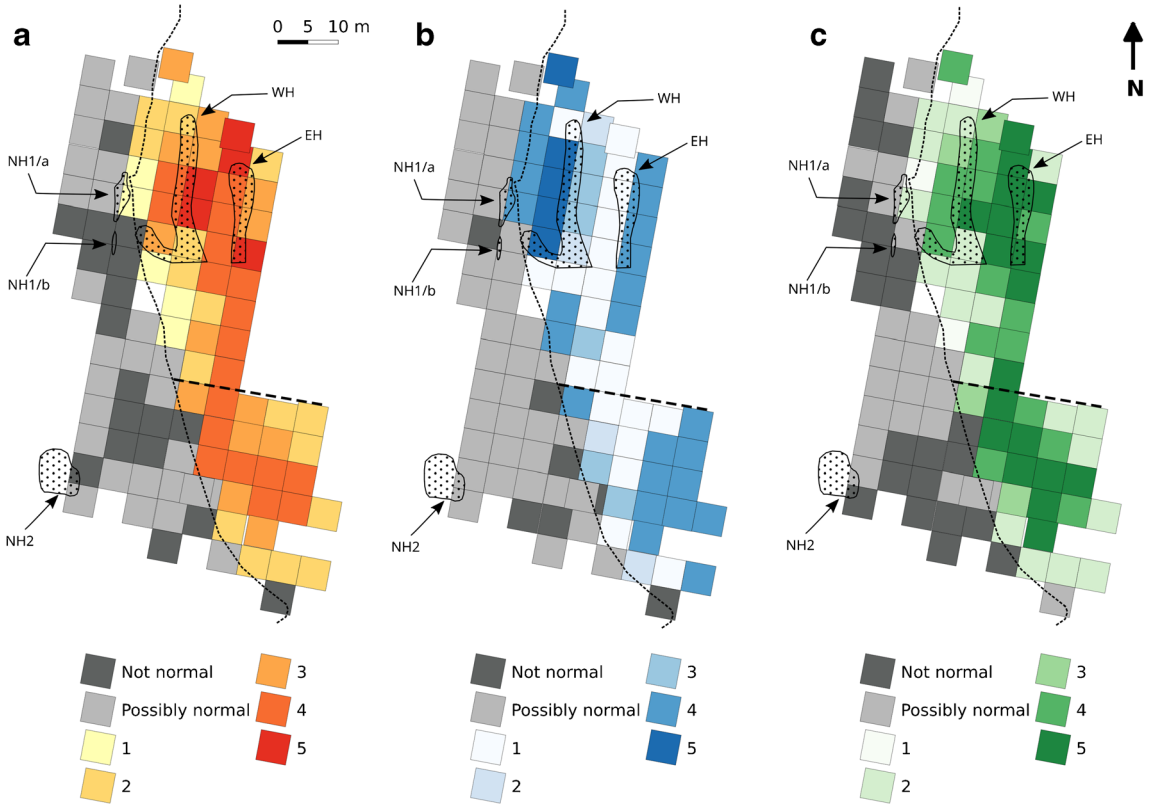

Fig. 10 Categories of normal distribution on the BA and the results of empirical probability density function on MB. **A** *x* displacement component. **B** *y* displacement component. **C** *z* displacement component. WH = western hollow after Bugya et al. (2011); EH = eastern hollow after Bugya et al. (2011); NH1/a and b = recent hollows on the northern part of BA; NH2 = recent hollow on the southern part of BA. Dashed lines indicate the border of southern and northern MB. To identify additional geomorphic details of the monitoring network, see Figs. 2B and 5D and H

Using the currently described field survey technique, we identified displacement trends of the MB, while measured movements were several orders of magnitude greater than the precision of the actual surveillance method. Moreover, field observations confirmed the opening of the crack and the displacement of the main block along the rupture surface. As a drawback, the classification of displacement components was based on somewhat subjective decisions. Moreover, unlike the other two components, clusters of the *y* component do not reflect obvious temporal changes. However, the currently employed methodology was appropriate for the identification of additional interior blocks and minor scarps and demonstrated the different displacement tendencies on the two sides of the MB. On the contrary, data from lost measurement points should be used with extreme caution. In spite of the clearly detected internal block of the MB according to the *y* component clusters, a further group of points with the same cluster value occurred around the margin of the southern and the northern MB. As a coincidence, this surface fragment lies in the latest crown of the rupture face, i.e. is found in front of the stable part of BA. As this part of the BA is characterised with points of normal distribution, it is free of any displacements. Hence, this block is assumed to be the elongation of the BA's stable zone on the MB. However, several metres of displacements occurred here disproving its stability. This kind of misinterpretation of clusters could happen if we disregard the loss of several points of this surface patch during the early measurement campaigns. Nevertheless, the mapping of point losses provided useful spatial information on the evolution on the deformational development of the escarpment.

In contrast to the MB, BA demonstrated permanent stability during field campaigns. Despite the introduced secondary base point and the destruction of the primary base point, precision of field survey remained almost constant with time. As device inaccuracies were greater than the actual range of surface displacements, therefore, we assumed stability for the entire BA. In contrary to Bugya et al. (2011), who used precise levelling on the background area of the 2008 landslide (northern part of MB in the present paper, see Fig. 13), measurement methods used in the current study were not sufficiently accurate to detect seasonal surface changes. Only normality testing of points indicated distinct spatial differences in point displacements on the SB.

Generally, points with non-normally distributed displacement values appeared more frequently on the northern and southern part of the BA. However, the abovementioned non-normal behaviour of points varied in accordance with the displacement components. Only a few points indicated the same (non-normally distributed data) behaviour regarding the three displacement components. Nevertheless, normality test results show similar spatial patterns (but not a perfect overlap) in the case of *x* and *y* displacement components, while the *y* component does not suggest distinct spatial differences. During the analysis of the MB, however, *z*

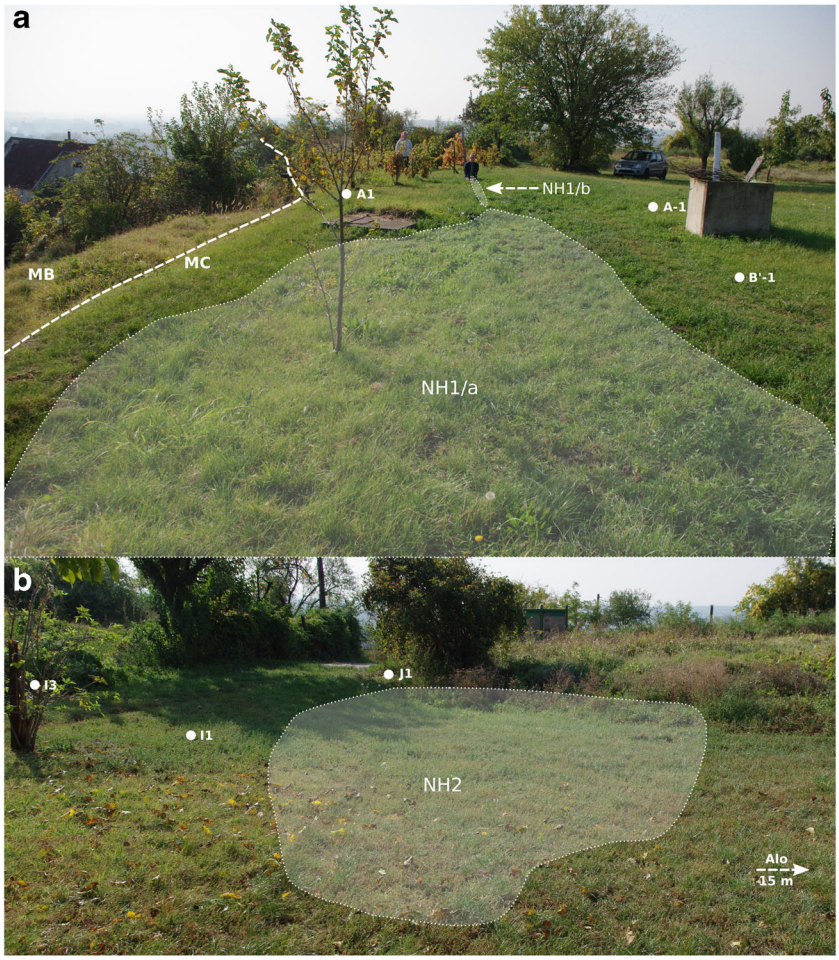

Fig. 11 View of the newly developed (recent) hollows (crown cracks) in October 2018. The hollows are bordered by dotted line. **a** Hollows (NH1/a, NH1/b) on the northern part of BA. **b** Hollow (NH2) on the southern part of BA. MB = moving block; MC = main crack. Further, letters indicate survey point locations. To identify additional geomorphic details of the monitoring network, see Figs. 2b and 5D and H

and *x* movement components were identified as the primary and secondary components of displacements.

The appearance of the new shallow hollows is the first visible sign of the displacements of the BA. However, unfortunately, there is no overlap between the point network and the hollows; hence, the connection of the non-normal distribution and hollow development cannot be fully validated. Formerly, we reported two shallow hollows from the research site (Bugya et al. 2011). They were formed on the northern MB almost in parallel with the recent scarp of the landslide (Fig. 13). They were up to 10 cm deep with a diameter of about 2 m. The western one was located among points A3–A5, B′3–B′5, C′3–C′5, D′3–D′5 and E′3–E′5, while the eastern one laid among points A7–A9, B′7–B′9 and C′7–C–9 (point names of the recent paper). Bugya et al. (2011) assumed hollows as the indicators of further displacements and disintegration processes within the MB. The formerly hidden crack of the western hollow (WH) was also partially excavated and identified by Szalai et al. (2014a); however, only a 'supposed crack line' was marked in the axis of the eastern hollow (cf. Fig. 7. in Szalai et al. 2014a). Later, Szalai et al. 2014b marked a 'coherent fracture zone' in the western hollow and fractures on the southern end of the eastern hollow (cf. Fig. 13; P2-P3 profiles in Szalai et al. 2014b). Subsequent minor crack and scarp development occurred only along the main axis of the WH. This crack development is in a good correspondence with our former expectations (Bugya et al. 2011). However, despite of the presence of EH and the fracture zone supposed by Szalai et al. 2014a, the entire eastern part of the northern MB (similarly to the whole southern MB) remained steady without any crack development and internal displacement. Considering the whole MB, successive crack development happened along only at a few sections of the fracture zones identified by Szalai et al. (2014a, b). Moreover, surface cracks appeared as curved lines on the surface, i.e. not along the previously expected straight lines. The recently investigated NH1/a and NH1/b hollows lie in the elongation of the rupture zone identified by Szalai et al. (2014b); however, there are no fracture zones marked by Szalai et al. (2014b) in the location of the hollow. Unfortunately, our present and former survey networks do not cover the area of hollow NH2. Despite the formerly mentioned facts, the hollows demonstrate the existence of displacements of the southern and northern part of BA, even if the point network does not overlap with them.

Points with possible normal distribution indicate almost constant normality with distinct spatial coverage in the central zone of the BA. Our findings therefore partly contradict to the results of

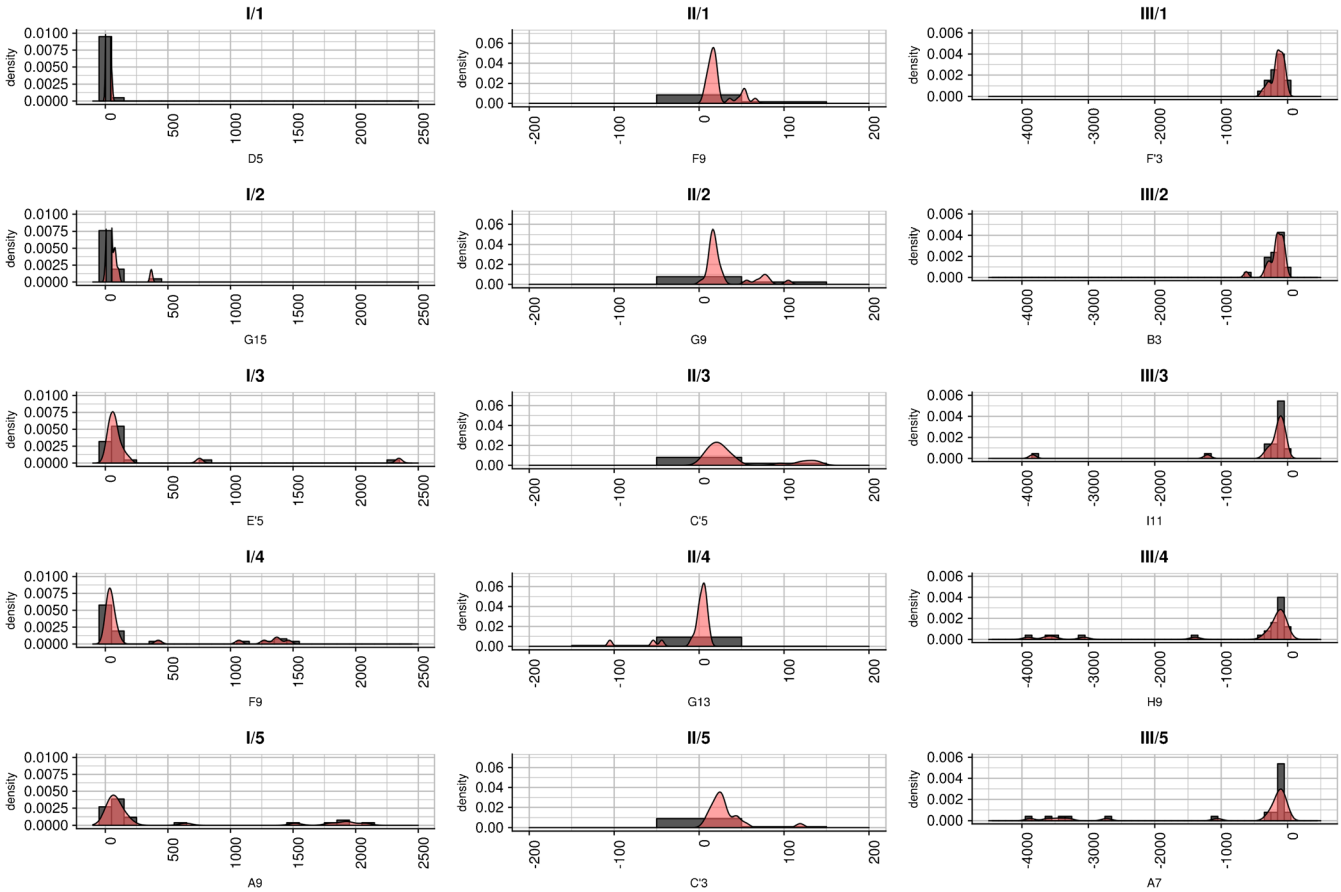

Fig. 12 Typical histograms and density plots of displacement clusters on the MB. I = clusters of x displacement component; II = clusters of y displacement component; III = clusters of z displacement component

Szalai et al. (2014b) as the authors assumed both fracture zones and a stable zone at the same site. However, we have not found any sign of surface displacements here, even 2 years after the termination of field campaigns.

The detected strong vertical subsidence of the MB is similar to the movement properties of former events (e.g. 2008 landslide). Those blocks appeared as surface steps with vertical, hanging slopes at various heights. They were not tilted backward to the high bluff neither destroyed by recent movements. These blocks drive the subsidence directions of recent block. On the contrary, the northern and southern parts of the recent MB moved in a different way indicating intense horizontal movements in the northern MB and vertical subsidence on the southern MB. Different movement patterns were also clearly reflected in the micromorphology of both parts of MB. Despite of the dissection of northern MB and the integrated subsidence of the southern MB, the main feature of the recent movement is the subsidence along a sharp dip angle, without a backward tilt of the MB head. Backward tilt of the block should be remarkable in the early phase of the sliding, and it could indicate a concave and shallow slip surface of the process. However, if the slip surface is deep enough, the backward tilt of the block appears only during the late development stage of the sliding.

The bottom of the by-channel of the Danube was already uplifted during the 2008 landslide event, and thereafter it functioned as a narrow floodplain. Additionally, a slight uplift of the floodplain and the river bed at the toe of the landslide has also been observed, simultaneously with the subsidence of the MB from 2011 onward. Nevertheless, the lateral erosion of the river removed the tip of the landslide away at a rate identical to the rate of displacement. Hence, the only consequence of displacements was a formation of a slight bulge, essentially a transverse ridge on the foot of the landslide, on the floodplain. The bulk of the landslide did not reach the surface and did not cause any damage here. In addition, flowering trees (willows, *Salix* sp.) of the floodplain did not suffer any visible damage or distortion (e.g. reaction wood development, decay or metabolic disorder) due to displacements, which suggests that the bulk of the landslide moved under the root zone.

The deposition of the landslide material caused further visible changes along the eastern bank of the peninsula. Here, the growth of the peninsula is directed to the east. It is clearly seen that two distinct surfaces (transverse ridges) with an escarpment of 2 to 3 m were formed during the displacements on the eastern bank of the peninsula. Firstly, the peninsula could be interpreted as the foot and toe (zone of deposition) of a deep-seated rotational slide. In this case, landslide material was sliding along a concave slip (rupture) surface underground, and the toe of the landslide slowly emerged in the Danube. This type of rotational slide should indicate the gradual uplift of the peninsula.

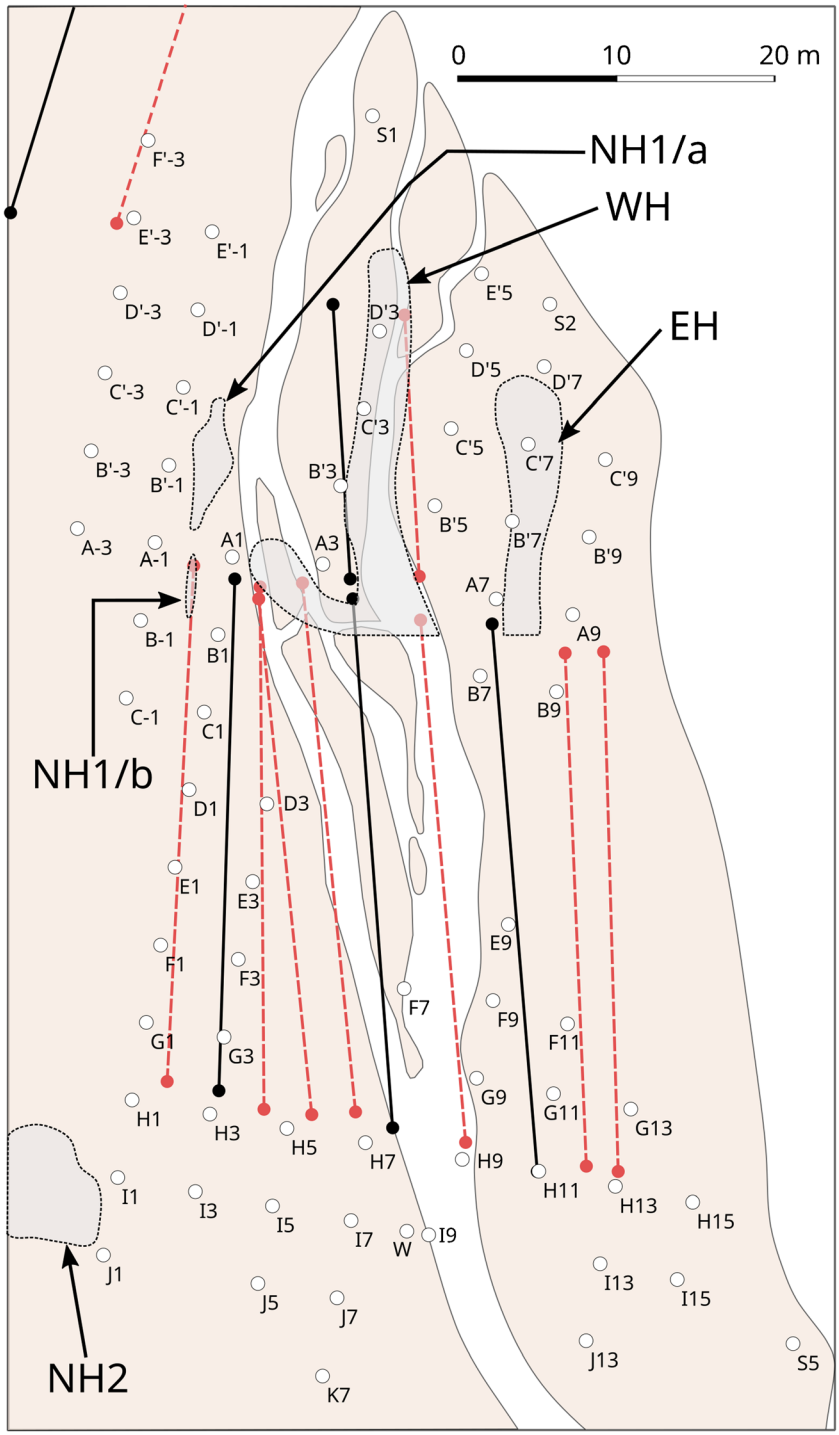

Fig. 13 Crack system of the landslide. WH = western hollow after Bugya et al. (2011); EH = eastern hollow after Bugya et al. (2011); NH1/a and b = recent hollows on the northern part of BA; NH2 = recent hollow on the southern part of BA; black line = stable zones according to Szalai et al. (2014b); dotted red line = fracture zones according to Szalai et al. (2014b). Line endings represent fracture zones identified on profiles by Szalai et al. (2014b). To identify additional geomorphic details of the monitoring network, see Figs. 2b and 5D and H

However, the eastward growth of the peninsula and mainly the absence of its destructive uplift strongly suggest an underground extrusion of the landslide material across the riverbed of the Danube. A similar interpretation of the 2008 landslide was presented by Kraft (2011) and Oszvald (2011). However, no data is available on the subsurface conditions of the foreland of the high bluff. Hence, the existence and shape of a rupture surface remain debated.

Conclusion

We pointed out that the displacements on the study area can be clearly identified with the applied time- and cost-efficient method and the observed trends provide data on future displacement trends. Based on our measurements, the following conclusions have been drawn:

- The main displacement component of MB has been identified as a vertical subsidence. Separation of the individual blocks of the MB was possible based on this component.
- Measurement of the two other components was also carried out; however, it is questionable that these secondary components need to be measured for further analyses.
- Despite the measuring inaccuracies, below the measurement limits, movements of BA were also detected using the simple normality testing of point coordinates.
- The emergence of hollows, which could indicate local instabilities of the background area, did not directly lead to further crack development. We assume further movements on the southern and northern parts of the BA, while the central part of BA is considered stable on the long run.
- A model, simulating movement dynamics, was developed based on our field observations. Neither the disintegration and vertical movement of the MB nor the prevention efforts slowed the movements down. This implies that the overall dynamics of the moving block could be interpreted as lateral spreading
- The recent movements pose a permanent risk on the foreground; further disturbance of the high bluff will likely intensify the vertical displacements.

Acknowledgements

Authors are grateful to the Mayor's Office of Dunaszekcső and especially to János Pap for providing permanent access to the restricted area of the Castle Hill. Authors are also grateful for the two anonymous reviewers for useful suggestions and comments on the manuscript.

Funding information

Open access funding provided by University of Pécs (PTE). The project has been supported by the European Union, co-financed by the European Social Fund grant no. EFOP-3.6.1.-16-2016-00004 entitled by Comprehensive Development for Implementing Smart Specialization Strategies at the University of Pécs.

References

Angeli MG, Pasuto A, Silvano S (2000) A critical review of landslide monitoring experiences. Eng Geol 55:133–147

Arbanas SM, Arbanas Z (2014) Landslide mapping and monitoring: review of conventional and advanced techniques. In Proceedings of the 4th Symposium of Macedonian Association for Geotechnics. Skopje 57–72

Bányai L, MentesGy ÚG, Kovács M, Czap Z, Gribovszki K, Papp G (2014) Recurrent landsliding of a high bank at Dunaszekcső, Hungary: geodetic deformation monitoring and finite element modeling. J Geodynam 47:130–141

Bas HG (2000) The accuracy of using theodolite in close-range engineering measurements. International Archives of Photogrammetry and Remote Sensing. 33, Amsterdam

Bugya T, Fábián SÁ, Görcs NL, Kovács IP, Radvánszky B (2011) Surface changes on a landslide affected high bluff in Dunaszekcső (Hungary). Central European Journal of Geosciences 3:119–128

Carlà T, Macciotta R, Hendry M, Martin D, Edwards T, Evans T, Farina P, Intrieri E, Casagli N (2018) Displacement of a landslide retaining wall and application of an enhanced failure forecasting approach. Landslides. 15:489–505. https://doi.org/10.1007/s10346-017-0887-7

Carr AP, Blackley MWL (1986) Seasonal change in surface level of a salt marsh creek. Earth SurfProc Land 11:427–439

Casagli N, Frodella W, Morelli S, Tofani V, Ciampalini A, Intrieri E, Raspini F, Rossi G, Tanteri L, Lu P (2017) Spaceborne, UAV and ground-based remote sensing techniques for landslide mapping, monitoring and early warning. Geoenvironmental Disasters 4. https://doi.org/10.1186/s40677-017-0073-1

Chae BG, Park HJ, Catani F, Simoni A, Berti M (2017) Landslide prediction, monitoring and early warning: a concise review of state-of-the-art. Geosci J 21:1033–1070. https://doi.org/10.1007/s12303-017-0034-4

Corominas J, van Westen CJ, Frattini P, Cascini L, Malet JP, Fotopoulou S, Catani S, Van Den Eeckhaut M, Mavrouli O, Agliardi F, Pitilakis K, Winter MG, Pastor M, Ferlisi S, Tofani V, Hervás J, Smith JT (2014) Recommendations for the quantitative analysis of landslide risk. Bull EngGeol Environ 73:209–263

Fodor P, Kleb B (1994) Engineering geological problems in loess regions of Hungary. Quat Int 24:25–30

Franyó F, Chikán G, Koloszár L (2005) Magyarország földtani térképe [Geological maps of Hungary] Baja, L-34-62, 1:100000 Magyar Állami Földtani Intézet [Hungarian Geological Institute] Budapest

Garcia A, Hordt A, Fabian M (2010) Landslide monitoring with high resolution tilt measurements at the Dollendorfer Hardt landslide, Germany. Geomorphology 120:16–25

Grist MW (1991) Close range measurement using electronic theodolite systems. Photogrammetric Record 13:721–729

Guerriero L, Guadagno FM, Revellino P (2018) Estimation of earth-slide displacement from GPS-based surface-structure geometry reconstruction. Landslides. 16:425–430. https://doi.org/10.1007/s10346-018-1091-0

Guzzetti F, Reichenbach P, Cardinali M, Galli M, Ardizzone F (2005) Probabilistic landslide hazard assessment at the basin scale. Geomorphology. 72:272–299. https://doi.org/10.1016/j.geomorph.2005.06.002

Guzzetti F, Mondini AC, Cardinali M, Fiorucci F, Santangelo M, Chang KT (2012) Landslide inventory maps: new tools for an old problem. Earth Sci Rev 112:42–66

Hu S, Qiu H, Wang X, Gao Y, Wang N, Wu J, Yang D, Cao M (2018) Acquiring high-resolution topography and performing spatial analysis of loess landslides by using low-cost UAVs. Landslides 15:593–612. https://doi.org/10.1007/s10346-017-0922-8

Huang R, Jiang L, Shen X, Dong Z, Zhou Q, Yang B, Wang H (2018) An efficient method of monitoring slow-moving landslides with long-range terrestrial laser scanning: a case study of the Dashu landslide in the Three Gorges Reservoir Region, China. Landslides. 16:839–855. https://doi.org/10.1007/s10346-018-1118-6

Jaboyedoff M, Oppikofer T, Abellán A, Derron MH, Loye A, Metzger R, Pedrazzini A (2012) Use of LIDAR in landslide investigations: a review. Nat Hazards 61:5–28. https://doi.org/10.1007/s11069-010-9634-2

Joó I (1992) Recent vertical surface movements in the Carpathian Basin. Tectonophysics 202:129–134

Kertész Á, Schweitzer F (1991) Geomorphological mapping of landslides in Hungary with a case study on mapping Danubian bluffs. Catena 18:529–536

Kovács IP, Fábián SÁ, Radvánszky B, Varga G (2015) Dunaszekcső Castle Hill: landslides along the Danubian loess bluff. In: Lóczy D (ed) Landscapes and landforms of Hungary. Springer International, Cham, pp 113–120

Kovács IP, Bugya T, Czigány S, Defilippi M, Dobre B, Fábián SÁ, Lóczy D, Riccardi P, Ronczyk L, Pasquali P (2018) Monitoring landslides using C-band interferometry. A case study: Dunaszekcső landslide, Southern Transdanubia, Hungary. StudiaGeomorphologicaCarpatho-Balcanica 51-52:87–105

Kovács IP, Bugya T, Czigány Sz, Defilippi M, Lóczy D, Riccardi P, Ronczyk L, Pasquali P, (2019) How to avoid false interpretations of Sentinel-1A TOPSAR interferometric data in landslide mapping? A case study: recent landslides in Transdanubia, Hungary Natural Hazards https://doi.org/10.1007/s11069-018-3564-9

Kraft J (2011) Dunaimagaspartdunaszekcsőirészleténekrogyásossuvadásai [Landslides of the Danubian high bluff at Dunaszekcső]. In: Török Á, Vásárhelyi B (ed) Mérnökgeológia – Kőzetmechanika [Engineering geology and rock mechanics]. HantkenKiadó, Budapest pp 93–104
Lilliefors HW (1967) On the Kolmogorov-Smirnov test for normality with mean and variance unknown. J Am Stat Assoc 138:399–402
Liu S, Wang Z (2008) Choice of surveying methods for landslides monitoring. In Chen et al. (eds.) Landslides and engineered slopes. Taylor and Francis Group, London
Lóczy D, Balogh J, Ringer Á (1989) Landslide hazard induced by river undercutting along the Danube. In: Embleton C, Federici PR, Rodoli G (eds.) Geomorphological hazards. Supplements of GeografiaFisica e DinamicaQuaternaria 2: 5–11
Lóczy D, Fábián SÁ, Schweitzer F (2007) River action and landslides in Hungary. In: Basu SR, De Sunil KR (eds) Issues in geomorphology and environment. Calcutta, India, pp 1–15
Maček M, Petkovšek A, Bojan M, Mikoš M (2014) Landslide monitoring techniques database. Landslide science for a safer geoenvironment. https://doi.org/10.1007/978-3-319-04999-1_24
Moyzes A, Scheuer G (1978) A dunaszekcsőimagaspartokmérnökgeológiaivizsgálata [Engineering geology of high bluffs at Dunaszekcső].FöldtaniKözlöny [Bulletin of the Hungarian Geological Society] 108:213–226
Mozas-Calvache AT, Pérez-García JL, Fernández-del Castillo T (2017) Monitoring of landslide displacements using UAS and control methods based on lines. Landslides 14:2115–2128. https://doi.org/10.1007/s10346-017-0842-7
Oszvald T (2011) Földcsuszamlások. [Landslides] ÖnKor Kép:25–27
Pecoraro G, Calvello M, Piciullo L (2018) Monitoring strategies for local landslide early warning systems. Landslides. 16:213–231. https://doi.org/10.1007/s10346-018-1068-z
Pécsi M (1994) A landslide type occurring frequently along the loess bluff in the Hungarian Danube section. Quat Int 24:31–33
Pécsi M, Schweitzer F (1995) Thelithostratigraphical, chronostratigraphical sequence of Hungarian loess profiles and their geomorphological position. Loess inForm (Budapest) 3:31–61
Peppa MV, Mills JP, Moore P, Miller PE, Chambers JE (2016) Accuracy assessment of a UAV-based landslide monitoring system. The international archives of the photogrammetry, remote sensing and spatial information sciences, Volume XLI-B5, 2016 XXIII ISPRS Congress, 12–19 July 2016, Prague, Czech Republic 895-902
Reichenbach P, Rossi M, Malamud BD, Mihir M, Guzzetti F (2018) A review of statistically-based landslide susceptibility models. Earth Science Reviews. https://doi.org/10.1016/j.earscirev.2018.03.001
Savvaidis PD (2003) Existing landslide monitoring systems and techniques. In Proc. of the Conference from Stars to Earth and Culture, In honor of the memory of Professor Alexandros Tsioumis Thessaloniki, Greece: The Aristotle University of Thessaloniki, 242–258
Szabó J (2003) The relationship between landslide activity and weather: examples from Hungary. Nat Hazards Earth Syst Sci 3:43–52
Szalai S, Szokoli K, Metwaly M (2014a) Delineation of landslide endangered areas and mapping their fracture systems by the pressure probe method. Landslides. 11:923–932. https://doi.org/10.1007/s10346-014-0509-6
Szalai S, Szokoli K, Novák A, Tóth Á, Metwaly M, Prácser E (2014b) Fracture network characterisation of a landslide by electrical resistivity tomography. Nat Hazards Earth Syst Sci Discuss 2:3965–4010. https://doi.org/10.5194/nhessd-2-3965-2014
Uhlemann S, Smith A, Chambres J, Dixon N, Dijkstra T, Haslan E, Meldrum P, Merritt A, Gunn D, Mackay J (2016) Assessment of ground-based monitoring techniques applied to landslide investigations. Geomorphology 253:438–451
Újvári G, Mentes G, Bányai L, Kraft J, Gyimóthy A, Kovács J (2009) Evolution of a bank failure along the river Danube at Dunaszekcső, Hungary. Geomorphology 109:197–209
Újvári G, Molnár M, Novotny Á, Páll-Gergely B, Kovács J, Várhegyi A (2014) AMS ^{14}C and OSL/IRSL dating of the Dunaszekcső loess sequence (Hungary): chronology for 20 to 150 ka and implications for establishing reliable age-depth models for the last 40 ka. Quat Sci Rev 106:140–154
vanWesten CJ, Castellanos E, Kuriakose SL (2008) Spatial data for landslide susceptibility, hazards and vulnerability assessment: an overview. EngGeol 102:112–131
Zhao C, Lu Z (2018) Remote sensing of landslides – a review. Remote Sens 10. https://doi.org/10.3390/rs10020279

I. P. Kovács (✉) · **T. Bugya**
Department of GIS and Cartography, Institute of Geography and Earth Sciences,
University of Pécs,
Ifjúság u. 6., Pécs, 7624, Hungary
Email: vonbock@gamma.ttk.pte.hu

S. Czigány · **S. Á. Fábián** · **G. Varga**
Department of Physical and Environmental Geography, Institute of Geography and Earth Sciences,
University of Pécs,
Ifjúság u. 6., Pécs, 7624, Hungary

B. Dobre
Doctoral School of Earth Sciences,
University of Pécs,
Ifjúság u. 6., Pécs, 7624, Hungary

M. Sobucki
Department of Geomorphology, Institute of Geography and Spatial Management,
Jagiellonian University of Cracow,
Gronostajowa 7., 30-387, Cracow, Poland